A Case Study of the Error Growth and Predictability of a Meiyu Frontal Heavy Precipitation Event*

LUO Yu (罗 雨) and ZHANG Lifeng† (张立凤)

Institute of Meteorology, PLA University of Science and Technology, Nanjing 211101

(Received October 25, 2010)

ABSTRACT

The Advanced Regional Eta-coordinate Model (AREM) is used to explore the predictability of a heavy rainfall event along the Meiyu front in China during 3–4 July 2003. Based on the sensitivity of precipitation prediction to initial data sources and initial uncertainties in different variables, the evolution of error growth and the associated mechanism are described and discussed in detail in this paper. The results indicate that the smaller-amplitude initial error presents a faster growth rate and its growth is characterized by a transition from localized growth to widespread expansion error. Such modality of the error growth is closely related to the evolvement of the precipitation episode, and consequently remarkable forecast divergence is found near the rainband, indicating that the rainfall area is a sensitive region for error growth. The initial error in the rainband contributes significantly to the forecast divergence, and its amplification and propagation are largely determined by the initial moisture distribution. The moisture condition also affects the error growth on smaller scales and the subsequent upscale error cascade. In addition, the error growth defined by an energy norm reveals that large error energy collocates well with the strong latent heating, implying that the occurrence of precipitation and error growth share the same energy source—the latent heat. This may impose an intrinsic predictability limit on the prediction of heavy precipitation.

Key words: heavy precipitation, predictability, initial error, model error growth, AREM

Citation: Luo Yu and Zhang Lifeng, 2011: A case study of the error growth and predictability of a Meiyu frontal heavy precipitation event. *Acta Meteor. Sinica*, **25**(4), 430–440, doi: 10.1007/s13351-011-0404-1.

1. Introduction

It is widely accepted that the predictability of atmosphere is limited to a finite lead time due to the interior stochastic dynamics. The concept of limited predictability due to instability in dynamic systems was first introduced by Maxwell (1876). Thompson (1957) defined the atmospheric predictability as the sensitivity to initial uncertainties and model errors in numerical weather prediction (NWP).

The atmosphere possesses motions on many scales. The scale-dependence of predictability was validated in early studies by Lorenz (1969), who indicated that the mesoscale motions are less predictable than the synoptic- or planetary-scale motions. The great progress in computer technology allows skillful performance of the NWP models in predicting the synoptic-scale evolution of weather systems. However, NWP models still have difficulty in forecasting the "mesoscale details" that are of great concern to forecasters. This can be partially attributed to the imperfectness in numerical models, but the uncertainty in initial conditions is thought to be a key contributor. The numerical research focusing directly on mesoscale predictability began with Anthes et al. (1985), who found little divergence of simulations from different initial conditions in a limited-area mesoscale model. Such a slow growth of forecast divergence was subsequently proved to be the artificial results due to the strong numerical diffusion and fixed lateral boundary conditions (Errico and Baumhefner, 1987).

Recently, Zhang et al. (2002, 2003) found that the rapid growth of initial error and the attendant upscale error growth contaminated the mesoscale predictabil-

*Supported by the National Natural Science Foundation of China (40975031).

†Corresponding author: zhanglif@yeah.net.

(Chinese version published in Vol. 68, No. 3, 411–420, 2010)

ity of the snowstorm in January 2000 along the east coast of the United States, and the moist physics was identified to be responsible for this strong initial-condition sensitivity of the mesoscale forecast. These results from a single case study were subsequently generalized by Tan et al. (2004), who examined the error growth in an idealized moist baroclinic wave amplifying in a conditionally unstable atmosphere. Zhang et al. (2006) also investigated the mesoscale predictability of a warm-season flooding event with stronger convective instability but weaker baroclinic instability. The results deduced that convective instability determines the rapid initial error growth at smaller scales, while baroclinic instability affects the upscale energy transfer and the error growth at larger scales.

It can be generalized from the above studies that understanding of the initial uncertainty impact and the error-growth modality is of great importance for assessing the predictability of mesoscale systems, particularly with respect to the associated precipitation. Since the generation of heavy rainfall is closely related to atmospheric instability and incidentally to the atmospheric nonlinearity, the prediction in such an unstable flow regime thus becomes highly sensitive to the initial condition. For instance, investigations of the torrential precipitation in July 1998 over Wuhan in China (Yu et al., 2001; Bei and Zhao, 2002) emphasized the importance of high-quality initial condition to the successful prediction of this heavy rainfall case.

Being one of the deadliest and costliest natural hazards in China, flood events have resulted in great economic losses in the past decades, and accurate precipitation prediction is therefore economically invaluable. As the demand is increasing for more precise forecast in order to minimize losses due to heavy rainfall destruction, the investigation of the impact of initial uncertainty on precipitation predictability is imperative and will lay an essential foundation for skillful forecast. In this sense, the evolution of initial error growth and the associated mechanism in NWP of precipitation should be discussed and analyzed in detail. This paper explores the prediction of the heavy precipitation in July 2003 along the Meiyu front in China. It is organized as follows. Model description and experimental design are provided in Section 2. Sensitivity of prediction to initial data sources and initial uncertainties in different variables with different amplitudes is discussed in Section 3. The detailed modality of error growth and its relation to the development of precipitation are discussed in Section 4. The mechanism for error growth is analyzed in Section 5. Conclusions and discussion are given in Section 6.

2. Mode description and experimental design

The AREM (Advanced Regional Eta-coordinate Model) is used for this study. It is a mesoscale model using the limited area Eta-coordinate system that can accommodate steep terrains. This model is well modulated to the rainstorm numerical prediction in China (Yu and Xu, 2004; Yu et al., 2004).

The predictability of heavy precipitation along the Meiyu front in China from 0000 UTC 3 to 0000 UTC 4 July 2003 is investigated. All the numerical simulations cover the domain 15°–50°N, 90°–130°E with a 0.25° (about 37 km) horizontal resolution and 32 layers in the vertical. The cold-cloud explicit microphysical scheme, Betts convection adjustment scheme (Betts and Miller, 1986), non-local boundary layer scheme (Holtslag and Boville, 1993), Benjamin and Seaman's surface radiation parameter scheme (Berjamin and Seaman, 1985), and multi-stratification profile surface flux scheme are employed. The simulations are all initialized at 0000 UTC 3 July 2003 and integrated for 24 h with boundary conditions derived from 1°×1° final analysis data of NCEP.

A series of sensitivity experiments are designed to investigate the impact of initial conditions on the precipitation prediction. Brief descriptions of these experiments are given in Table 1.

It should be noted that the difference in each variable between the initial condition of Exp_STN and that of Exp_NCP has its magnitude much smaller than the associated variable itself. Such differences thus correspond to small perturbations. In this sense, Exp_T and Exp_UV can be equivalently regarded as adding small perturbations to the initial temperature-

Table 1. A list of the sensitivity experiments

Objective	Experiment	Description
Sensitivity to initial data sources	Exp_STN	Initial data derived from conventional observation and reanalyzed through the AREM objective analysis system
	Exp_NCP	Initial data derived from 1°×1° final analysis of NCEP and reanalyzed through the AREM objective analysis system
Sensitivity to initial uncertainties in thermodynamic variables	Exp_T	Same as Exp_STN, except that the initial temperature and moisture distributions are derived from 1°×1° NCEP data
Sensitivity to initial uncertainties in dynamic variables	Exp_UV	Same as Exp_STN, except that the initial horizontal winds are derived from 1°×1° NCEP data
Sensitivity to initial errors with different amplitudes	Exp_T1, Exp_T05, Exp_T01, Exp_T001	Same as Exp_STN, except for the addition of perturbations to initial temperature. Perturbation is defined by $T' = T_0 \cdot \mathrm{Rand}$, where T_0 is the amplitude and is set to 1, 0.5, 0.1, and 0.01 K respectively. Rand is a random number uniformly distributed within the interval –1 to 1
Contribution of initial error in rainfall area to the forecast divergence and effect of initial moisture condition on error growth	Exp_T01LP	Same as Exp_T01 but only perturbing the initial temperature in the rainfall area (31°–35°N, 113°–123°E)
	Exp50_T01LP	Same as Exp_T01LP except with the initial moisture being reduced by 50%
Impact of moist physics and the attendant latent heating on error growth	Expdry_T01LP	Same as Exp_T01LP except with the latent heating being turned off during the entire integration
	Expdryaf6h_T01LP	Same as Exp_T01LP but without the latent heating after 6-h integration

and wind fields, which will not bring serious side effects to the balance among initial variables.

3. Analysis of the sensitivity experiments

3.1 Sensitivity to initial data sources

The 24-h accumulated precipitation valid at 0000 UTC 4 July is presented in Fig. 1. The observation (Fig. 1a) shows that the west-east oriented rainband has three rainfall centers located near (33°N, 114°E), (33.5°N, 117°E), and (34°N, 120°E), respectively. The simulated results show that Exp_NCP almost fails to predict the heavy rainfall episode (Fig. 1c), while Exp_STN performs well in simulating both the spatial distribution of the rainband and the location of rainfall centers (Fig. 1b). To further quantify the precipitation prediction from these two experiments, TS scores with thresholds of 5, 10, 25, and 50 mm are calculated over the rainfall area. The result indicates that Exp_STN is more skillful than Exp_NCP for each threshold (Table 2). The strong sensitivity of precipitation prediction to initial data sources is thus validated. It is also suggested that the conventional observation is a better approximation to the initial condition, which is essential in the successful prediction of this heavy rainfall event.

Because the hourly precipitation can reflect some mesoscale details of the heavy rainfall process, a further comparison is conducted between Exp_STN and Exp_NCP for hourly precipitation prediction over the severe rainfall center near (33.5°N, 117°E) in Anhui. Figure 2 shows that Exp_NCP produces much weaker precipitation and fails to simulate the "single peak" exhibited in observation. Exp_STN, which is skillful in 24-h accumulated precipitation prediction, reproduces the drastic intensifying trend of rainfall and has its maximum hourly precipitation comparable to the observation although its peak time lags the observation. This indicates the difficulty in predicting the mesoscale details of the heavy rainfall in operational forecast.

Next, the specific difference between the initial condition of Exp_STN and that of Exp_NCP that results in the large forecast divergence of precipitation is examined. Figure 3 shows the latitude-height sections of the equivalent potential temperature (θ_{se}) along

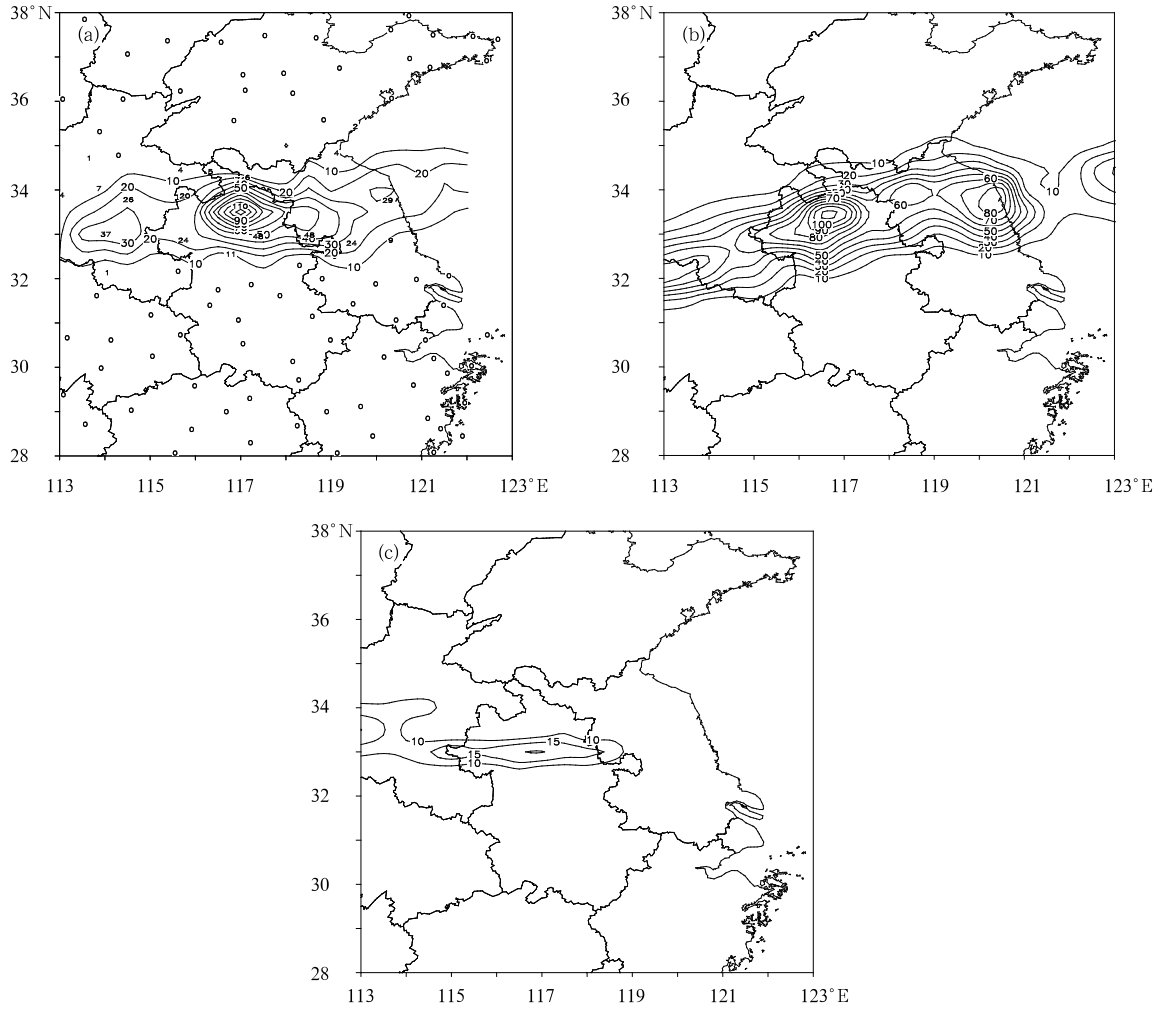

Fig. 1. 24-h accumulated precipitation (mm) valid at 0000 UTC 4 July 2003 from (a) observation, (b) EXP_STN (control simulation), and (c) EXP_NCP.

Table 2. TS scores for EXP_STN and EXP_NCP

Threshold	EXP_STN	EXP_NCP
5 mm	0.54	0.29
10 mm	0.42	0.17
25 mm	0.21	0.0
50 mm	0.042	0.0

117°E at the initial time. It is found that the θ_{se}-isolines in Exp_NCP (Fig. 3a) are almost vertical over the rainfall area, which corresponds to the neutral stratification or weak convective instability. In contrast, the isolines in Exp_STN present a warm moist center with high θ_{se} at lower level, and the dry cold air prominently intrudes at about 550 hPa. Such a stratification indicates strong convective instability and is more favorable for intensive convection and the subsequent precipitation, which consequently determines the precision of precipitation prediction. Moreover,

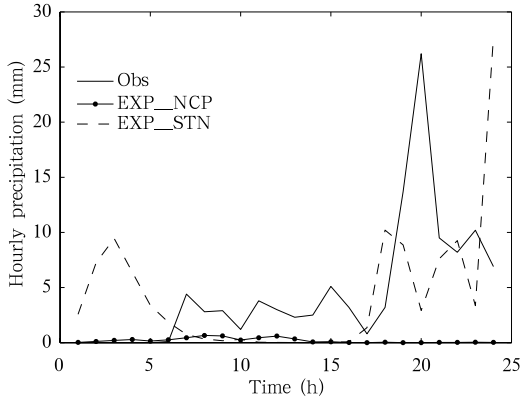

Fig. 2. Hourly precipitation (mm) of the rainfall center in Anhui from 0000 UTC 3 to 0000 UTC 4 July.

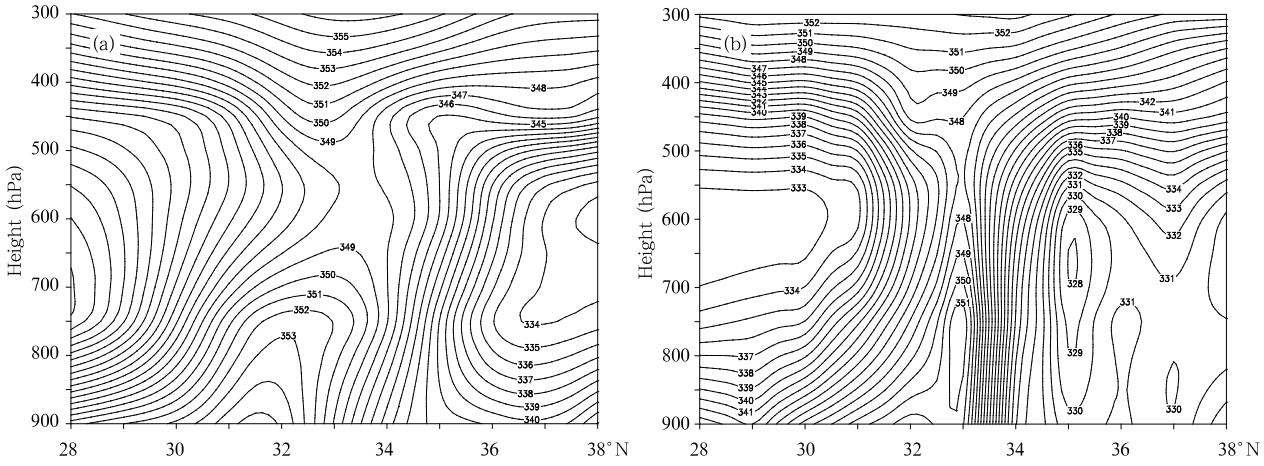

Fig. 3. Latitude-height sections of θ_{se} (K) along 117°E of (a) EXP_STN and (b) EXP_NCP at the initial time.

Exp_STN produces stronger initial convergence (divergence) at lower (upper) level over the rainfall area (figure omitted), which is more conducive to the triggering of strong convection and the generation of heavy precipitation.

3.2 Sensitivity to initial errors with different amplitudes

The above results suggest that Exp_STN performs better than Exp_NCP in simulating the spatial distribution and temporal variation of this precipitation episode. Thus, Exp_STN can be regarded as the control simulation (hereafter CNTL) and the following sensitivity experiments will be based on and compared with CNTL unless otherwise specified. In addition, the perturbation or error referred to hereafter is thus defined as the difference from CNTL. This methodology has been proved effective in discussing the predictability problems by Bian and Yang (2003).

We begin with the comparison between Exp_T and Exp_UV. The results (figure omitted) indicate that Exp_T has a larger RMSE in the precipitation forecast during the entire integration. This implies that the prediction of the heavy rainfall is more sensitive to initial uncertainties in thermodynamic variables. In comparison, the initial moisture is perturbed in another experiment, and the results (figure omitted) show that the initial uncertainties in the temperature field still lead to a larger forecast error than that of the simulation with the initial moisture perturbation. In this sense, the initial temperature is chosen to be the sensitive variable that is to be perturbed and a series of sensitivity experiments (i.e., Exp_T1, Exp_T05, Exp_T01, and Exp_T001) are conducted to investigate the forecast sensitivity to the initial temperature errors with different amplitudes. The initial temperature perturbation is independent at each grid point and each model level.

Figure 4 shows the time series of precipitation forecast RMSEs resulted from initial temperature perturbations with different amplitudes. It is found that the simulation with a smaller initial temperature perturbation gives a faster error growth rate. For instance, the magnitude of the forecast error due to 0.01-K initial temperature perturbation is comparable to that due to 1-K initial perturbation by 24 h. This

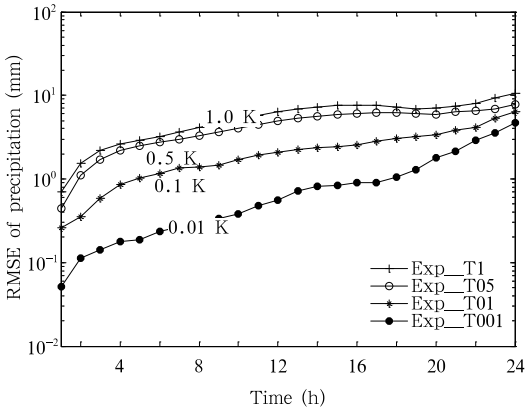

Fig. 4. Time series of RMSE of precipitation forecast from different experiments.

implies that a sufficiently small initial error in the temperature field could also result in noticeable forecast errors. Actually, for 24-h accumulated precipitation, the case of 0.01-K initial temperature perturbation leads to an unappreciable displacement of the rainband, but the corresponding localized precipitation bias reaches a maximum of 25 mm at mesoscale, indicating the complete displacement of the local rainfall centers. That is to say, a very small (e.g., 0.01 K) initial error is not negligible.

To further illustrate the influence of initial error amplitude on precipitation prediction, we introduce an integrated norm for error (difference), namely, the domain-integrated difference total energy (DTE), as defined by Zhang et al (2003):

$$\mathrm{DTE} = \sum(\delta u_{i,j,k}^2 + \delta v_{i,j,k}^2 + \frac{C_p}{T_r}\delta T_{i,j,k}^2), \qquad (1)$$

where δu, δv, and δT are the differences in wind components and temperature between CNTL and the perturbed simulation, $T_r = 287$ K is the reference temperature, $C_p = 1004$ J kg^{-1} K^{-1} is the specific heat at constant pressure, and i, j, and k run over the horizontal points and vertical layers. Figure 5 presents the time series of DTE at 500 hPa. During the initial stage (about 5 h), the smaller the initial error is, the faster it grows. Particularly, DTE in Exp_T001 grows most rapidly after 16 h, and its magnitude is comparable to that in Exp_T1. Thus, the smaller perturbations (errors) tend to grow more rapidly and maintain the growth over a longer period. The DTEs corresponding to different initial errors span a range of values on the same order of magnitude by 24 h rather than on the four orders of magnitude shown initially.

The dependence of error growth rate on the initial error amplitude indicates that the mechanism for error growth is nonlinear, which is consistent with the physical arguments by Lorenz (1969). For the initial small-amplitude errors (e.g., the case of 0.01-K initial perturbation), the effect of diffusion is weaker and smaller than the effect of nonlinearity in the initial stage. The smaller perturbation consequently grows faster and steadily throughout the entire forecast. Therefore, such forecast sensitivity to sufficiently small errors in the initial condition highlights the importance of high-quality initial data to fine precipitation prediction and hence calls for the improvement in observation instrument precision and the development of data assimilation techniques.

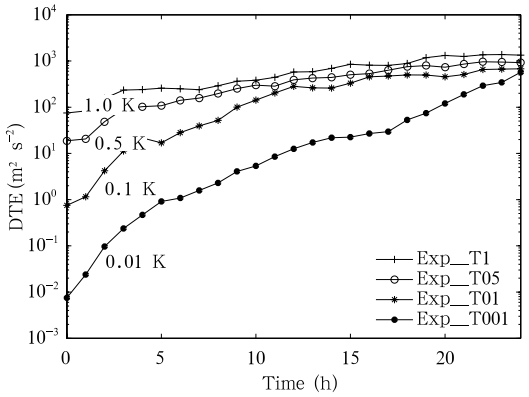

Fig. 5. Time series of DTE (m^2 s^{-2}) at 500 hPa from different experiments.

4. Modality of error growth and its relation to precipitation development

4.1 Evolution and propagation of error growth

Since the forecast divergence due to initial error growth should be examined not only in terms of the error magnitude amplification, but also in terms of the error-growth evolution and propagation, the detailed modality of error growth is described and discussed in this section.

Figure 6 presents the evolution of temperature difference at 500 hPa between Exp_T01 and CNTL. Generally, the significant error growth first appears in local patches and subsequently spreads over a larger area. Combined with the evolvement of the precipitation episode, it is of great interest that the evolution of error growth exhibits three distinctive stages. The first stage lasts from 0 to 6 h (Fig. 6a), during which the initial random perturbation has decayed everywhere except for a small region with prominent precipitation. Moreover, the area with localized error growth moves eastward as the associated rainfall area in north Anhui gradually moves eastward and lingers near north Jiangsu, with the fact that the error increases as the precipitation strengthens. During the second stage (from 9 to 15 h; Figs. 6b, c), as the rainfall near north Jiangsu declines, the error growth

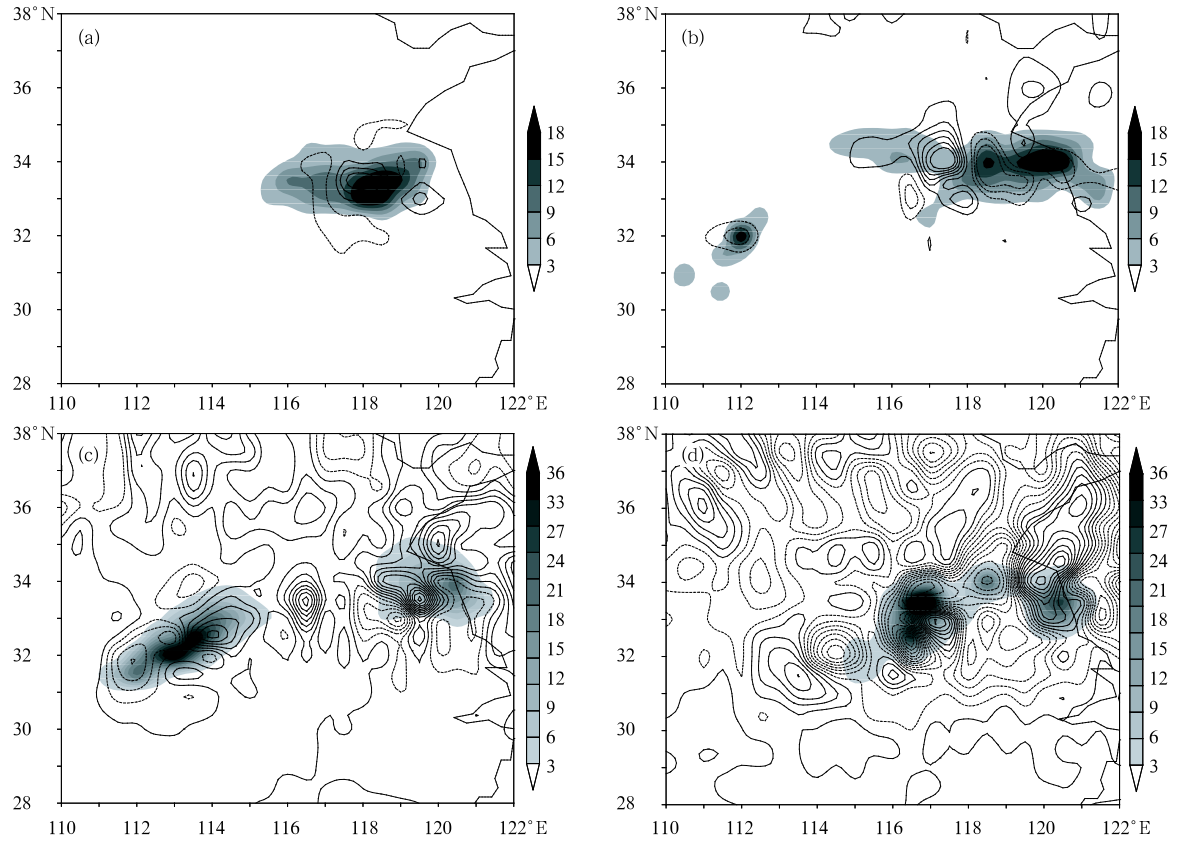

Fig. 6. 500-hPa temperature difference between Exp_T01 and CNTL (contoured every 0.1 K; dashed for negative; shaded for CNTL 3-h accumulated precipitation in mm) valid at (a) 6 h, (b) 9 h, (c) 15 h, and (d) 24 h.

over the corresponding region slows. Meanwhile, a meso-β rain cell with a spatial scale of about 200 km appears in southwest Henan and it increases both in its precipitation amount and the spatial coverage, leading to the formation of a northeast-southwest oriented rainband. In phase with this rainfall development, the error growth over the associated area increases in both its magnitude and areal extent, with the larger error collocated well with the rainfall center. In the final stage (15 to 24 h; Fig. 6d), the newly-born rainband near Henan maintains its intensity as it rapidly moves eastward to north Anhui, and it merges with the previous declining rainfall-area over north Jiangsu where the reinforcement of precipitation occurs consequently. In accordance with the evolution of precipitation, the area with significant error growth in southwest Henan moves eastward along the same path as the moving rainband, and the previously slowing error growth near north Jiangsu begins to amplify further.

The correspondence between the evolution of error growth and the evolvement of the precipitation episode can therefore be reflected in Fig. 6. In terms of the above multi-stage error growth, larger differences are concentrated in the vicinity of the rainband along the Huaihe River basin during 0 to 15 h, thus the first two stages can be concluded to be the period characterized by localized error growth. The error increases prominently in both its magnitude and areal extent after 15 h in the subsequent period. Meanwhile, the drastic intensification of precipitation also appears after 15 h. This implies the important role of the precipitation evolvement in affecting the error growth and its propagation.

The above behavior of error growth is manifested not only in temperature but also in wind fields. Since the difference of wind velocity can be regarded as the proxy of difference kinetic energy, the associated multi-stage error growth in wind also reflects the

error-energy evolution. Besides, similar error-growth modality can be observed in Exp_T1, Exp_T05, and Exp_T001. It therefore suggests that since sufficiently small errors in the initial condition are inevitable, such a transition of error growth from local patches to larger coverage ultimately contaminates the mesoscale forecast and leads to the predictability limit of heavy precipitation.

4.2 Correspondence between error growth and the precipitation episode

It has been revealed in this study that the optimal error growth appears near the rainfall area and that the area coverage of significant error growth varies in phase with the evolution of precipitation. Therefore, the rainfall area is the sensitive region for error growth. It can be deduced that the initial uncertainty in the rainfall area is an important and direct contributor to large forecast divergence. To validate this, sensitivity experiments Exp_T01LP and Exp50_T01LP are designed, where the latter aims at reducing the initial moisture to delay the triggering of convection and the generation of precipitation. It should be noted that the error (perturbation) referred to in this section for Exp_T01LP denotes the difference between Exp_T01LP and CNTL, while that for Exp50_T01LP denotes the difference between Exp50_T01LP and the corresponding dry control simulation with initial moisture reduced by 50% but with unperturbed initial temperature.

The comparison between Exp_T01LP and Exp50_T01LP reflects the correspondence between the meridional propagation of error growth and the evolution of precipitation. Clearly, although the initial uncertainties appear in the rainfall area, the error growth also exhibits the transition from localized patches to wide clumps with a larger areal extent and presents a strong northward propagation (Fig. 7a). This results in the error growth north to the rainband reaching a larger amplification, consistent with the facts in Fig. 6d. As the precipitation episode is delayed and declined due to the reduced initial moisture (Fig. 7b), the associated significant error growth in Exp50_T01LP appears later than that in Exp_T01LP, and both the magnitude and the meidional propagation extent are greatly weakened. The close correspondence between the error growth amplification and the precipitation intensity further indicates the rainfall-dependent nature of the error growth. Considering the unavoidable initial error and the relationship between error growth and precipitation development, the sophisticated numerical model inevitably "favors" the forecast divergence due to initial error growth and hence leads to the prediction limit of precipitation.

In order to further quantify the variation of error growth, power-spectrum analysis of DTE is performed for the above two experiments. For Exp_T01LP (Fig. 8a), the DTE spectrum peaks at the wavelength of 300 km during the first 12 h, which corresponds to the period of localized error growth. After 15 h, 300-km and smaller-scale components of the DTE spectrum

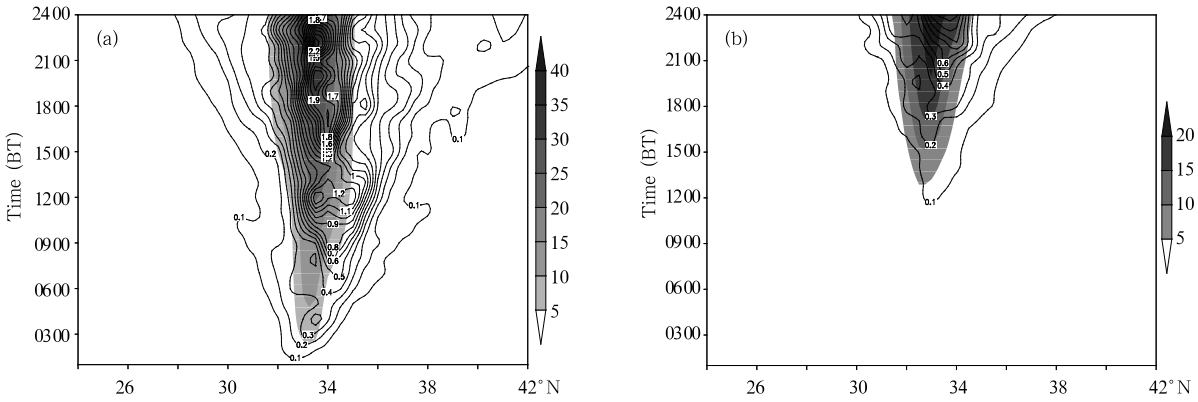

Fig. 7. Latitude-time section averaged within 113°–123°E for the wind velocity difference (contoured every 0.1 m s^{-1}) and the accumulated precipitation (mm; shaded) on 3 July 2003 in (a) Exp_T01LP and (b) Exp50_T01LP.

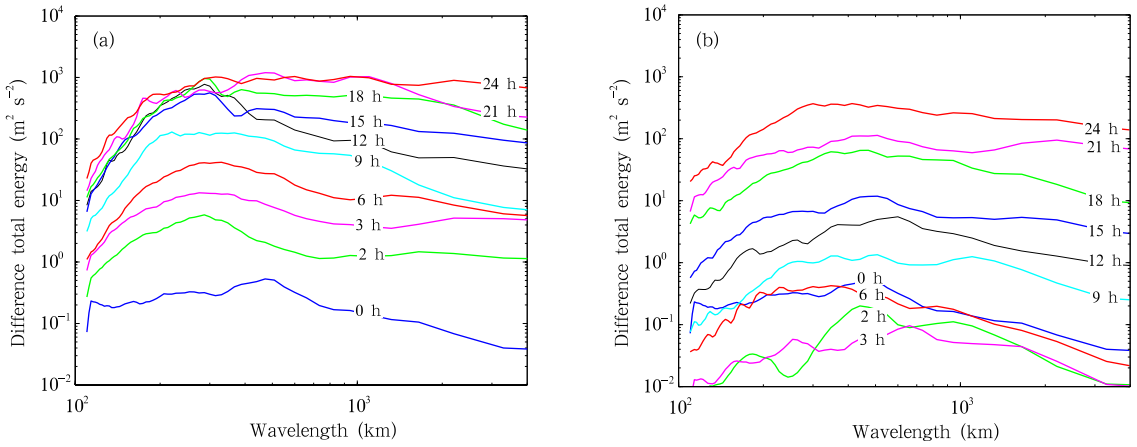

Fig. 8. Power spectrum of DTE at 500 hPa for (a) Exp_T01LP and (b) Exp50_T01LP.

become saturated while the larger-scale errors grow steadily. The peak of the spectrum thus migrates from smaller (500–600 km by 21 h) to larger scale (around 1000 km by 24 h). This validates the upscale cascade of the error growth. Considering the results in Section 4.1, the modality of rainfall-dependent error growth can be further elucidated as follows. Over the first 15 h, the error grows rapidly and reaches saturation on smaller scale, which indicates the localized growth period. During the remaining time, both the scale of the error variation and its areal extent increase, which indicates the error spreading period. Thus, such upscale error growth contaminates the mesoscale forecast and limits the precipitation predictability.

Figure 8b shows the DTE spectrum for Exp50_T01LP. It is found that the DTE on all scales decreases over the first 2 h and this is most prominent at the wavelength of 200–300 km. The DTE growth relative to the initial time does not appear until 9 h. Clearly, as the reduced initial moisture delays and attenuates the precipitation episode, the associated error growth begins at a later time with a smaller magnitude. Moreover, the optimal error growth on the smaller scale (wavelength) becomes less significant. Thus, the change of heavy rainfall due to reduced moisture consequently affects the magnitude, propagation, and scale variation of the error growth.

5. Error growth mechanism

It has been proved in previous sections that the error growth is closely related to the precipitation evolvement, but the key physical processes, i.e., the mechanism for error growth, is not clear. Obviously, moist physics is essential in triggering convection and associated precipitation. Besides, the feedback by latent heat release is also crucial to the maintenance of heavy rainfall. In an attempt to further investigate the role of moist physics and the attendant latent heating in producing significant error growth, two "fake dry" experiments are performed, in which the latent heating of condensation is set to zero for a certain lead time.

In Expdry_T01LP, the latent heating is turned off throughout the 24-h integration. This results in much smaller error growth with a reduced propagation extent compared with Exp_T01LP (figure omitted). Figure 9 shows that in the absence of latent heating, the growth of DTE over the rainfall area is greatly reduced during the first 5 h and the subsequent slow DTE growth gradually reaches saturation. While in Expdryaf6h_T01LP, the latent heating is not allowed after 6 h. This causes the errors to quickly decay and dissipate after 6 h (figure omitted), and the associated DTE enhances rapidly before 6 h, then decreases quickly, and finally becomes saturated (Fig. 9).

A further comparison of the DTE growth among Exp_T01LP, Exp50_T01LP, Expdry_T01LP, and Expdryaf6h_T01LP is shown in Fig. 9. It reveals that affluent initial moisture corresponds to rapid error growth in the initial stage and larger amplification of error growth by the end of the simulations

(Exp_T01LP versus Exp50_T01LP). The comparison between two moist simulations (Exp_T01LP and Exp50_T01LP) and two fake dry experiments (Expdry_T01LP and Expdryaf6h_T01LP) indicates that latent heating is responsible for the significant error growth and is able to sustain the error growth after the difference energy has already been produced. In addition, Fig. 10 shows the spatial distributions of DTE and latent heat at 24 h. It is found that the areas of large DTE collocate well with the strong latent heating. Since DTE defines the error growth in an energy norm and the feedback by latent heating is essential in maintenance of heavy rainfall, it can be concluded that the error growth and the occurrence of precipitation share the same energy source—the latent heat. This indicates that the unstable flow regime favorable for heavy rainfall also corresponds to the rapid error growth in precipitation prediction. In this sense, the forecast divergence due to error growth associated with the interior thermodynamic and dynamic instability of the atmosphere is inevitable and the predictability of heavy precipitation is inherently limited.

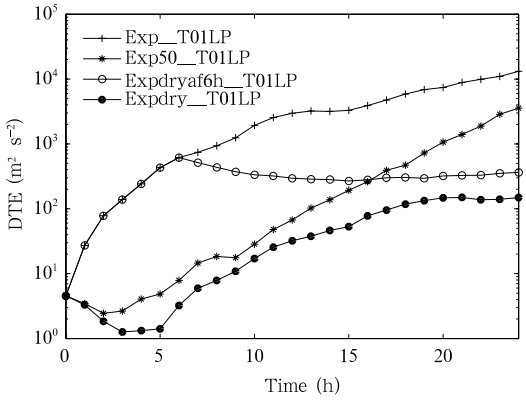

Fig. 9. Time series of DTE in the rainfall area from different experiments.

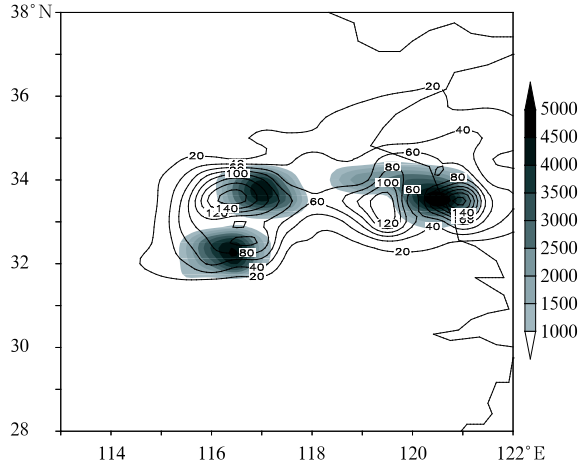

Fig. 10. Spatial distribution of DTE (contours; $m^2\ s^{-2}$) from Exp_T01LP and latent heat (shaded; J) from CNTL valid at 24 h.

6. Conclusions and discussion

Based on a case study, this paper analyses the sensitivity of precipitation prediction to initial conditions. The influence of initial error amplitude on the prediction and the detailed modality of error growth associated with the heavy rainfall evolvement are investigated and discussed. The results have identified the key physical process and mechanism for the significant error growth and also validated the inherent difficulty in fine-scale precipitation prediction. The main conclusions are as follows.

The prediction of this heavy rainfall event is highly sensitive to the initial uncertainties in thermodynamic variables. The error growth rate increases as the initial error amplitude decreases, which indicates that the mechanism for error growth is nonlinear. After a certain lead time, the forecast divergence due to growth of initial smaller-amplitude errors is comparable to that due to larger initial errors.

The significant error growth concentrates in the vicinity of the rainfall area, with the areas of large forecast difference collocated well with the intensive rainfall centers. Particularly, the evolution of error growth is in phase with the evolvement of precipitation. The attendant error-growth transition from local patches to wide spreading clumps leads to the forecast divergence over larger areas. This consequently limits the mesoscale predictability of heavy precipitation.

The close correspondence between error growth and precipitation evolvement also validates the important contribution of initial uncertainties over rainfall area to the precipitation forecast divergence. The rainfall-dependent error growth presents an upscale cascade and has its optimal amplification on a certain spatial scale (wavelength) during the forecast.

The moist physics and the attendant latent heating are responsible for the significant error growth.

The areas with large error energy collocates well with the strong latent heat release, implying that the latent heating serves as the energy source for the error growth. As the feedback by latent heating is also essential to sustained heavy rainfall, it can be deduced that the error growth and the occurrence of precipitation share the same energy source—latent heating.

The conclusions here are in general agreement with previous studies (Zhang et al., 2003; Tan et al., 2004; Bei and Zhang, 2007) though this study focuses on the relationship between the error growth modality and precipitation evolvement. It is of interest that the amplification and propagation of error growth is closely related to the intensity and evolution of rainfall process. Particularly, latent heating is found to be the shared energy source for error growth and the occurrence of precipitation. As sufficiently small errors is inevitable in the initial condition, their growth associated with moist process and the attendant latent heating thus impose an intrinsic predictability limit on heavy rainfall forecast. Besides, the faster growth rate of smaller initial errors may be worth further investigations.

Presumably, these conclusions imply that the fine prediction of precipitation is inherently difficult. However, this does not mean there is nothing that can be done to improve the forecast skill. Implementation of high-resolution observation network and development of efficient data assimilation techniques are ways to make the initial condition a better approximation to the true atmosphere and to improve the forecast skill for a finite time in NWP. In addition, another alternative is to develop probabilistic or ensemble forecasting schemes for the quantitative estimation of precipitation predictability.

REFERENCES

Anthes, R. A., Y. H. Kuo, D. P. Baumhefner, et al., 1985: Predictability of mesoscale atmospheric motions. *Advances in Geophysics*, **28**B, 159–202.

Bei Naifang and Zhao Sixiong, 2002: Effect of initial data and physical processes on the heavy rainfall prediction in July 1998. *Climatic and Environmental Research*, **7**(4), 386–396. (in Chinese)

Bei, N., and F. Zhang, 2007: Impacts of initial condition errors on mesoscale predictability of heavy precipitation along the Mei-Yu front of China. *Quart. J. Roy. Meteor. Soc.*, **133**, 83–99.

Berjamin, S. O., and N. L. Seaman, 1985: A simple scheme for objective analysis in curved flow. *Mon. Wea. Rev.*, **113**, 1184–1198.

Betts, A. K., and M. J. Miller, 1986: A new convective adjustment scheme. Part I: Observational and theoretical basis. *Quart. J. Roy. Meteor. Soc.*, **112**, 677–691.

Bian Jianchun and Yang Peicai, 2003: Some remarks on the predictability of atmospheric processes. *Plateau Meteorology*, **22**(4), 315–323. (in Chinese)

Errico, R., and D. P. Baumhefner, 1987: Predictability experiments using a high-resolution limited area model. *Mon. Wea. Rev.*, **115**(2), 488–504.

Holtslag, A. M., and A. Boville, 1993: Local versus nonlocal boundary-layer diffusion in a configuration for a large-scale model. *Quart. J. Roy. Meteor. Soc.*, **122**, 689–719.

Lorenz, E. N., 1969: The predictability of a flow which possesses many scales of motion. *Tellus*, **21**(3), 289–307.

Maxwell, J. C., 1876: *Matter and Motion.* Dover, New York, 136 pp.

Tan, Z., F. Zhang, R. Rotunno, and C. Snyder, 2004: Mesoscale predictability of moist baroclinic waves: experiments with parameterized convection. *J. Atmos. Sci.*, **61**, 1794–1804.

Thompson, P. D., 1957: Uncertainty of initial states as a factor in the predictability of lagre scale atmospheric flow patterns. *Tellus*, **9**(3), 275–295.

Yu Rucong, Xu Youping, and Xia Daqing, 2001: The bursting evolution of "98.7" Wuhan torrential rain simulated by REM. *Chinese Science Abstracts*, **7**(3), 362–365. (in Chinese)

—— and ——, 2004: AREM and its simulations on the daily rainfall in the summer of 2003. *Acta Meteor. Sinica*, **62**(6), 715–724. (in Chinese)

——, Xue Jishan, Xu Youping, et al., 2004: *Advanced Regional Eta-Coordinate Numerical Heavy-Rain Prediction Model (AREM) Systems (AREMS).* China Meteorological Press, Beijing, 11–42. (in Chinese)

Zhang, F., C. Snyder, and R. Rutunno, 2002: Mesoscale predictability of the "surprise" snowstorm of 24–25 January 2000. *Mon. Wea. Rev.*, **130**, 1617–1632.

——, ——, and ——, 2003: Effects of moist convection on mesoscale predictability. *J. Atmos. Sci.*, **60**, 1173–1185.

——, A. M. Odins, and J. W. Nielsen-Gammon, 2006: Mesoscale predictability of an extreme warm-season rainfall event. *Wea. Forecasting*, **21**(2), 149–166.